PROCEEDINGS OF SPIE

SPIEDigitalLibrary.org/conference-proceedings-of-spie

Detection and identification of plastics using SWIR hyperspectral imaging

Mehrubeoglu, Mehrube, Van Sickle, Austin, Turner, Jeffrey

Mehrube Mehrubeoglu, Austin Van Sickle, Jeffrey Turner, "Detection and identification of plastics using SWIR hyperspectral imaging," Proc. SPIE 11504, Imaging Spectrometry XXIV: Applications, Sensors, and Processing, 115040G (22 August 2020); doi: 10.1117/12.2570040

SPIE.

Event: SPIE Optical Engineering + Applications, 2020, Online Only

Detection and identification of plastics using SWIR hyperspectral imaging

Mehrube Mehrubeoglu*[1a], Austin Van Sickle[b], Jeffrey Turner[2a]
[1]Hyperspectral Optical Property Instrumentation (HOPI) Laboratory, Department of Engineering
[2]Laboratory for Microbial and Environmental Genomics, Department of Life Sciences
[a]Texas A&M University-Corpus Christi, 6300 Ocean Dr., Corpus Christi, TX 78412, USA
[b]Surface Optics Corporation, 11555 Rancho Bernardo Rd., San Diego, CA 92127, USA

ABSTRACT

Most plastics are typically transparent in the visible spectral range, rendering them challenging to detect using silicon-based vision sensors. In this work a SWIR hyperspectral imaging system is used to collect the SWIR hyperspectral signatures as well as spatial information of a variety of plastics outdoors to test this technology for plastic debris detection and identification in future marine and environmental applications. In this study, hyperspectral imaging data have been collected from plastic samples including CPVC, PVC, LDPE, HDPE, PEEK PETG, PC, PP, PS, and Polyester in a natural environment. The data is acquired using a SWIR hyperspectral imaging system sensitive to 900 - 1700 nm wavelength range. Four spectral indices based on labeled spectral signatures have been identified and used as features to separate plastic materials and for classification of pixels. Semantic segmentation based on plastic materials is achieved in an independent scene with multiple plastic samples using shortest Euclidean distance to labeled feature cluster centers through multi-variate data analysis. The results show the capability of this technology and technique to detect and classify different plastics in natural environments under different light conditions.

Keywords: hyperspectral imaging, SWIR hyperspectral imaging system, NIR imaging spectroscopy, macroplastics, microplastics, plastic debris detection, identification of plastics, semantic segmentation

1. INTRODUCTION

Detecting plastic waste and debris is an on-going environmental and health concern. Plastic pollution, especially in aquatic environments, is widely regarded as an environmental crisis. In 2010 alone, 275 million metric tons (MT) of plastic waste was generated and 4.8 to 12.7 million MT of this waste are expected to have entered the oceans[1]. A recent report from the Ellen MacArthur Foundation estimates that ocean plastic debris will outnumber fish by the year 2050[2]. In particular, microplastics have received significant attention due to their global abundance and potential for negative ecological and human health outcomes[3,4]. For example, microplastic exposure was shown to induce gene transcription, immune response, and behavioral changes in zebrafish[5]. Similarly, microplastic exposure was shown to induce intestinal barrier disfunction and bile acids metabolism disorder in mice[6]. Accurate monitoring and risk assessment will require overcoming the fundamental challenges of detecting and identifying microplastics. Advanced methodologies are needed to quickly and accurately analyze large numbers of heterogeneous samples at the micro-scale in a high-throughput manner.

The detection and identification of microplastic debris is commonly a three-step process: 1) Bulk or concentrated water samples are passed through a membrane filter to collect microplastic debris, 2) Non-synthetic debris (i.e., natural particulate organic matter) is digested using hydrogen peroxide, and 3) Particles and fibers are detected and identified visually using microscopy and/or chemically using spectroscopy (e.g., FTIR and Raman) or chromatography (e.g., pyrolysis GC/MS and HPLC)[7]. Microscopy is simple and affordable, but limitations include a high possibility of false positives. Previous studies[8] have shown that rates of false positive identification can exceed 70%. In the example of microplastic fibers, which are especially difficult to distinguish from natural fibers, another study demonstrated that more than 98% of fibers were falsely identified[9]. Spectroscopy is more accurate, but limitations include the lengthy time for sample analysis. The coupling of micro-FTIR with semi-automatic mapping technology reduces analysis time to approximately nine hours per filter but this only permits the analysis of two samples per day[10]. Pyrolysis GC/MS is advantageous in that it permits the analysis of bulk samples, but the destructive nature of thermal analysis prevents further characterization[11].

Imaging Spectrometry XXIV: Applications, Sensors, and Processing, edited by Emmett J. Ientilucci, Pantazis Mouroulis, Proc. of SPIE Vol. 11504, 115040G · © 2020 SPIE
CCC code: 0277-786X/20/$21 · doi: 10.1117/12.2570040

Hyperspectral imaging (HSI), or imaging spectroscopy, is a promising alternative method where membrane filters are imaged and processed by multivariate data analysis to identify and characterize plastic debris. In contrast to previous spectroscopic methods that require the time-consuming analysis of individual particles, HSI allows for the rapid analysis of many particles simultaneously. Working with heterogeneous environmental samples, Karlsson showed that hyperspectral image analysis detected a higher number of particles than conventional microscopic analysis[12], and Shan demonstrated that HSI correctly identified more than 97% of microplastic particles[13]. Collectively, the increased sensitivity reduces the risk of underestimation, the increased accuracy reduces the risk of false positives, and the less time-consuming analysis permits high-throughput analysis.

In this study, short-wave infrared (SWIR) HSI is used to investigate the separability of thirteen different macroplastic samples of dimensions 3" x 4". The purpose of this investigation is to identify these plastic materials based on their spectral characteristics under natural light in a representative environment that they are expected to be found in the form of debris. Although multiple groups have been studying plastics detection and identification using hyperspectral imaging, this study includes more varieties of plastics than have been found in the literature.

1.1 Plastic Pollutants in the Environment

The most common plastics include Polypropylene (PP), Low Density Polyethylene (LDPE), High Density Polyethylene (HDPE) the three of which represent over 56% of produced plastics as the polyolefin (PO) family, followed by polyethylene terephthalate (PET), Polyvinyl Chloride (PVC), and Polystyrene (PS)[14,15]. PET can be flexible or thoroughly rigid, and is highly durable, which is why it is used in containers for water, soft drinks, cooking oil, packaging and freezable food trays, as well as polar fleece, among other uses. HDPE can withstand high temperatures as well as chemicals, and is therefore used for containers of cleaning solutions, soaps, food and drinks, as shopping and freezer bags in addition to pipes, bottle caps, insulation material, helmets, and other products which are all recyclable. PVC is widely used due to its practical material properties and affordability. PVC can be made into clothing, including leather-like materials, and is commonly found in signage, furniture, tubing, plumbing pipes, vinyl flooring, cables, cleaning solution containers, and water bottles[14,16]. LDPE shows itself in everyday use as shopping bags, containers, parts for machines, drink cartons, hardware casings, as well as laundry bags among other products. Polystyrene is used as Styrofoam, disposable razors, and CD cases[16,17]. PP appears in rugs, ropes as well as bottle caps[16].

1.2 Hyperspectral Imaging for Characterization of Plastics

Multiple research groups have investigated the use of SWIR hyperspectral imaging for the detection of both macro and microplastics. At the macro level, Balsi *et al.*[17] use SWIR spectral imaging in the range 900 nm – 1700 nm for spectral characterization of polymers including Polyethylene (PE) of the three types (HDPE, LDPE, and Linear Low Density Polyethylene (LLDPE), as well as PP, PVC, PS, Polycarbonate (PC), PET, and Polylactic acid (PLA). This spectral range is also referred to NIR in the literature. The authors use a device based on two-linear-spectrometer principles for spectral characterization. The authors identify the absorption peaks for the different plastics using continuum removal method. Hibbitts *et al.* use hyperspectral imaging to isolate two effective infrared bands for discriminating plastic objects such as fiberglass, styrene, PP, and polyesters by taking advantage of the first harmonic of the vibrational carbon-hydrogen absorption band between 1650-1750 nm[16]. The authors identify the band ratio 1540:1710 (bands in nm) as an effective ratio to detect plastics with a two-camera system optimized around these wavebands.

Serranti *et al.* describe SWIR hyperspectral imaging in the range 1000 – 2500 nm combined with chemometrics to identify polymers in samples collected from different marine environments[15]. The authors show principal component analysis (PCA) score plots for first and second principal components and use partial least-squares discriminant analysis to differentiate among polymers such as PP, PE, and expanded Polystyrene. In a parallel study, Serranti describes the potential of SWIR HSI for monitoring marine plastic waste[18].

In an earlier 2013 study, Bonifazi *et al.* lay the foundation for quality control of plastic recycling using a hyperspectral imaging system they developed for PO materials in plastic waste streams[19]. The authors use a SWIR HSI system coupled with multivariate analysis for spectral analysis and classification for this particular application. Moroni *et al*. also describe the application of HSI in recycling for the separation of PET and PVC in different phases of their life cycle[20]. The group tests visible (400-1000 nm) and SWIR (900-1700 nm) range and concludes that the visible-range wavebands were not effective in differentiating PET and PVC due to the visible range being dependent on colors. The authors use the ratio of

absorbance values at 1656 nm and 1712 nm to separate PET and PVC. In their more recent publication, Moreno and Mei describe plastics as contaminants in the recycling process that need to be separated[21]. This time the authors describe the use of hyperspectral imaging to separate PET, PS and PLA samples at their different life cycles (from virgin to urban plastic waste). The authors make use of distinctive absorption bands as spectral indices (ratio or difference of two bands) for the three materials together with correlation matrix analysis for a real-time application. After continuum removal, the authors identify the spectral index of 1170:1650 (ratio 1) to separate PET from PLA and PS, and 1160:1140 (ratio 2) to separate PLA from PS after that, using a decision tree procedure. In another recycling application, Caballero *et al*. describe the use of HSI to separate polymers with flame retardants to allow grouping of plastics with the same polymer type and additive content necessary for recycling[22]. The authors implement chemometrics solutions for classification, including partial least-square discriminant analysis, decision tree, and hierarchical model, achieving a sensitivity of higher than 90% with discriminant analysis method that the authors report are valuable findings for plastics and waste management industries.

At the micro level, Karlsson *et al.* investigate HSI and data analysis for detection and identification of plastic contamination in seawater filtrates in simulated samples to test the application of SWIR HSI in the detection of microplastics down to 300 μm in size[12]. Zhang *et al.* describe the use of hyperspectral imaging in detection of microplastic polymer pellets of PE, PS, PET, PP and PC in sizes ranging from 0.1 to 1 mm[23]. The authors incorporate support vector machine classification scheme for differentiating the polymers. Chuczko *et al*. explore use of neural networks for detecting microplastics in hyperspectral images obtained from natural environments[24]. They train their algorithm with 1000 samples, and test with 100 samples, achieving 95% accuracy of classification in their controlled experiments. They conclude that use of machine learning techniques is promising for the future of microplastic classification.

In this study we investigate spectral signatures of thirteen different plastic samples using SOC710-SWIR hyperspectral imaging system[25]. Using band ratios as spectral indices, the tested materials are detected and their separability demonstrated in a scatter plot representing each material. The list of tested plastic samples and methods for hyperspectral image acquisition, visualization and analysis are presented in the next section. Images of plastic samples as well as spectral and spatial data from the SOC710-SWIR HSI system is shown in Section 3. Plastic sample separation and identification results and analysis are presented in Section 4. Conclusions are summarized in Section 5.

2. METHODOLOGY

Table 1 summarizes the thirteen different plastic samples analyzed in this study. These materials ranged in their chemical makeup as well as color.

Table 1. Plastic materials[26,27] investigated using SOC710-SWIR HSI

Sample	Material	Acronym	Color
1	High-Density Polyethylene	HDPE	black
2	High-Density Polyethylene	HDPE	white
3	High-Temperature Chlorinated Polyvinyl Chloride	High-Temperature CPVC	gray
4	Kydex Acrylic Polyvinyl Chloride	Kydex Acrylic PVC	gray
5	Low-Density Polyethylene	LDPE	white
6	Polycarbonate	PC	clear
7	Polyetheretherketone	PEEK	tan
8	Polyethylene Terephthalate Modified with CHDM	PETG	clear
9	Polyester [unspecified]	Polyester	white
10	Polypropylene	PP	white
11	Polystyrene	PS	amber
12	Polystyrene	PS	white
13	Polyvinyl Chloride	PVC	black

2.1 Equipment and Collection of Hyperspectral Data Cubes

Hyperspectral data cubes were collected by a SWIR hyperspectral imaging (HSI) system (SOC710-SWIR, Surface Optics, San Diego, CA) that covered the spectral range from in 900 – 1700 nm, with spatial size of 640 x 512 pixels and 288 spectral bands[25]. Each pixel represented a bit depth of 12 bits. The system's image acquisition parameters were optimized for the sample and calibration panel. Calibration panel is necessary because the measurements were taken outside in natural sunlight, which varies based on the time of day and seasons. Calibration panel allows the normalization of data across multiple lighting conditions, where plastic debris would usually be found, as opposed to repeatable controlled laboratory environments. The calibration panel, a gray panel used as a reference, displays low reflectivity (about 18%). The gray calibration panel is advantageous over highly reflective white calibration panels, since the gray panel allows increased light reflectance from the tested sample without saturating the reference or calibration panel. The measured reflectance, in turn, is a modified reflectance, R_M, that can be higher than the reference panel in some instances, calculated as:

$$R_M(x,y,\lambda) = I_i(x,y,\lambda) / I_g(\lambda), \quad (2)$$

where (x,y) represents the 2D spatial location of the pixel within each hyperspectral image frame, and λ refers to a single spectral band at which the reflectance is to be computed. $I_i(x,y,\lambda)$ represents the observed value as a single data point (voxel) in the hyperspectral data cube corresponding to the tested sample in the scene located at pixel (x,y) in the 2D image frame at waveband λ. $I_g(\lambda)$ is the spatial average of observed values for the gray panel at spectral band λ. $I_g(\lambda)$ was obtained from the same scene as the sample, but can be acquired independently near the same time of the experiments. The dark response is ignored in the computation of R_M above.

2.2 Spectral and Spatial Data Visualization

Each pixel's spectrum represents the (mixed) material spectral signature observed at the spatial location of the pixel. Spatial visualization, on the other hand represents the scene with the objects' physical and relative placement in space, more specifically, the 2D projection of the 3D scene. Spatial information at different spectral bands can be extracted from hyperspectral data cubes as image frames corresponding to a narrow wavelength range based on the manufacturer's system and internal calibration. Combining spectral and spatial data produces information that may not be attainable by spectral or spatial information alone, such as the material at a given location in the scene. During testing, spectral signatures for each plastic sample were obtained from the hyperspectral data cubes based on the spatial information locating the sample in the scene. After data processing, a semantically segmented image is created as described next, demonstrating the identified location of plastic samples. MATLAB 2017a was used for all data processing post hyperspectral data acquisition.

2.3 Material Classification and Semantic Mapping

Four spectral indices were identified for detection, separation, and semantic segmentation and mapping of the plastic samples. First, each sample was imaged using SWIR HSI separately for spectral labeling. Testing was achieved from an independent HSI scene captured on a different day with multiple plastic samples in the scene. The spectral indices were chosen from spectral bands as band ratios demonstrating the highest separability among the thirteen plastics' spectral signatures represented as modified reflectance explained in a previous work[28]. Eight spectral band pairs were chosen that corresponded to 985 nm and 1041 nm; 1139 nm and 1223 nm; 1419 nm and 1461 nm; and 1574 nm and 1670 nm. Band ratios were computed as ratio_1 = 985:1041, ratio_2 = 1139:1223, ratio_3 = 1419:1461, and ratio_4 = 1574:1670 and corresponded to the values (observations) at each band.

The band ratios were used in scatter plots to demonstrate material separability visually. Mean cluster values were computed from 500 spectra for each plastic material. Euclidean distance was computed between cluster means and spectral indices obtained from each of the unlabeled pixels in a new hyperspectral image for semantic segmentation and mapping. Euclidean distance is calculated for multivariate data as:

$$D_E = [\,(x_1 - x_{r1})^2 + (x_2 - x_{r2})^2 + (x_3 - xr_3)^2 + \ldots + (x_n - x_{rn})^2\,]^{1/2}, \quad (2)$$

where D_E is the Euclidean distance from the unknown sample spectral indices used as features, or representation of spectra, to the cluster center for labeled plastic spectral indices. $X = [x_1, x_2, x_3, \ldots, x_n]$ is the n-variate feature vector (n=4 in this study) for each spectrum. $X_r = [x_{r1}, x_{r2}, x_{r3}, \ldots, x_{rn}]$ represents the n-variate feature vector for the cluster center belonging to labeled plastics. D_E is computed separately for the cluster center of each of the thirteen plastics. If the shortest Euclidean distance between the tested pixel's spectral indices and cluster means was found below a distance threshold (acceptably close), the plastic label was assigned to that pixel. Otherwise, the pixel was not labeled: $I_i(x,y) \in S$ if $D_E < t$, where

S = {1, 2, 3, …, 13} where each number in S represents a plastic material label. *t* is the threshold value above which the pixel is not labeled as one of the plastics.

A semantic map was created based on the match between the tested pixel's feature vector of spectral indices, and each of the thirteen labeled plastics' mean feature vector (cluster center) of the same spectral indices.

3. DATA

In this section, the samples and experimental data are presented. Figure 1 displays each of the investigated plastic samples as a hyperspectral image frame extracted from a spectral band from the hyperspectral images. Each scene contains a single plastic sample. The plastic sample appears in front of the calibration panel. The SWIR hyperspectral image is acquired outdoors under natural light. The displayed image frames are extracted from SWIR hyperspectral data cubes at waveband 1139 nm (frame 85) for demonstration purposes. Sample numbers are as described previously in Table 1.

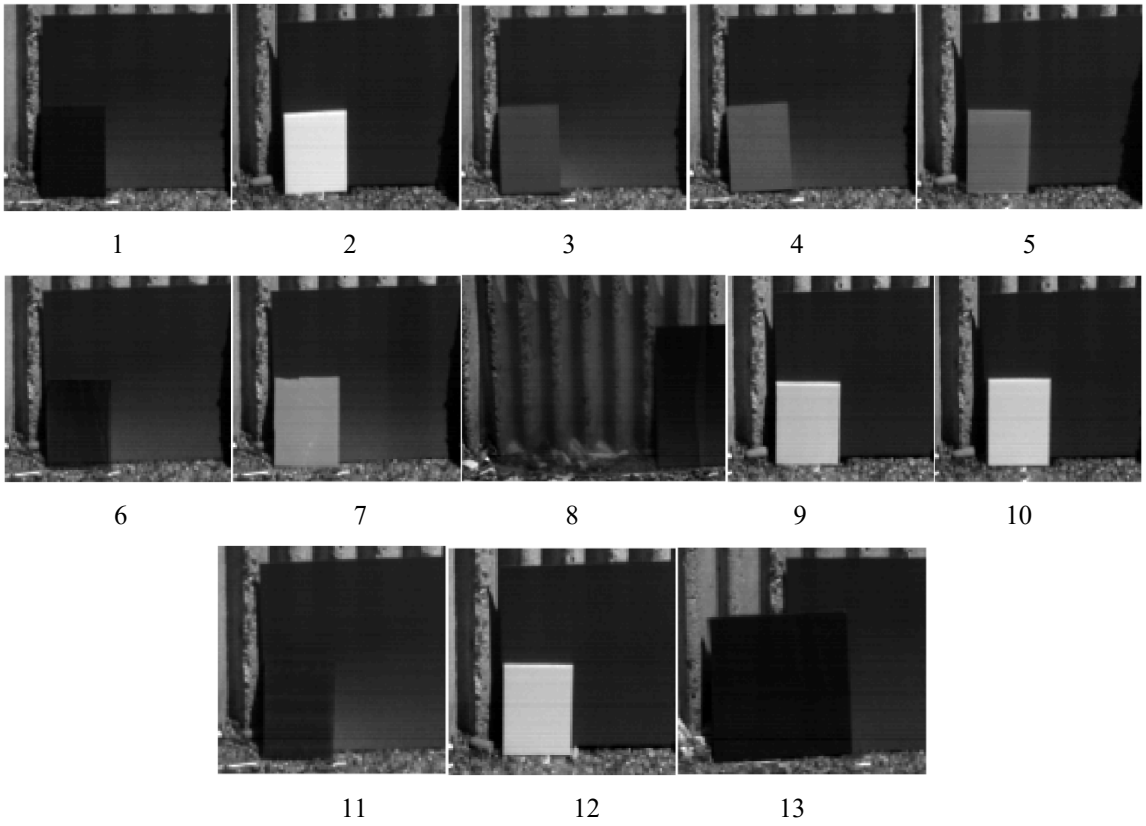

Figure 1. Single plastic samples in front of gray calibration panel acquired outdoors (frame 85 corresponding to ~1139 nm wave band) and used for spectral feature selection. (Plastic samples, in listed order, 1: HDPE (black), 2: HDPE (white), 3: High-Temperature CPVC (gray), 4: Kydex Acrylic PVC (gray), 5: LDPE (white), 6: PC (clear), 7: PEEK (tan), 8: PETG (clear), 9: Polyester (white), 10: PP (white), 11: PS (amber), 12: PS (white), 13: PVC (black)).

Figure 2 displays multiple plastic samples in a single scene collected on a different date and time. This scene is used for testing, and mapping plastic identification results. We note that Polyethylene (PE) was not included in the training due to the unavailability of this sample during the feature extraction period. In addition, this scene is missing the PS (amber) sample.

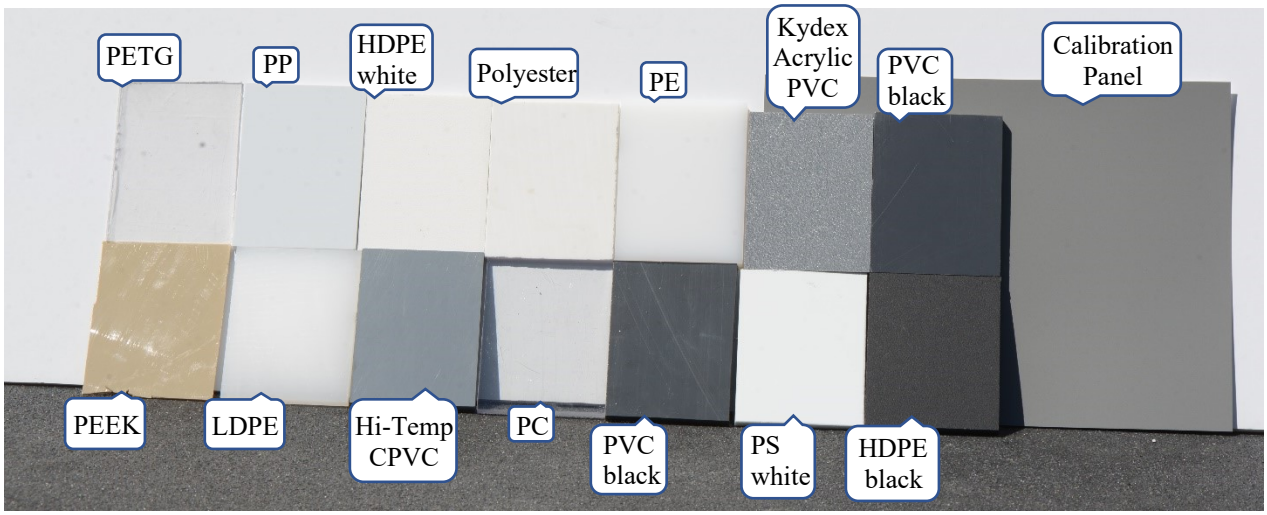

Figure 2 Color image of tested plastic samples used in classification. (Cal Panel: Calibration Panel; PE: Polyethylene) (SWIR hyperspectral image of the same scene was obtained with the SWIR HSI system separately).

Average modified spectra for plastic samples are displayed in Figure 3. Each spectrum represents the average of 500 spectra from the corresponding material. Since the reference or calibration panel is a gray (and not white) panel, modified reflectance is higher than the reference for most of the materials, and lower or comparable in selected samples such as HDPE black, PETG clear, and PVC black, for the majority of the spectra.

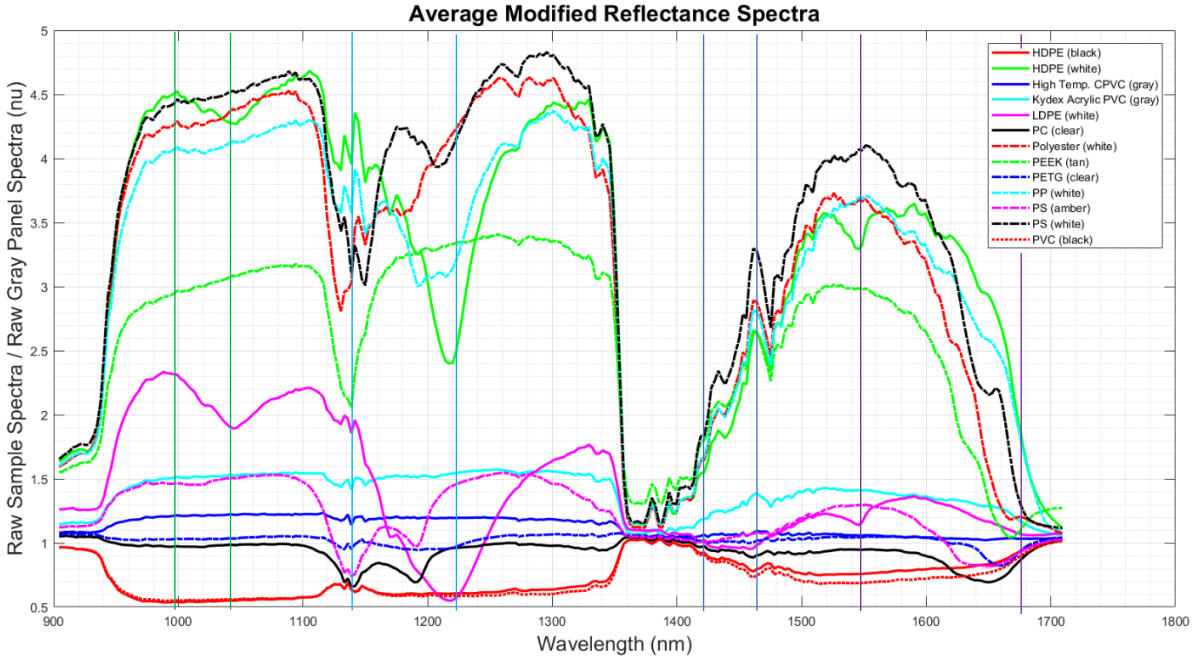

Figure 3. Average modified reflectance spectra using gray calibration panel.

4. RESULTS

Figure 4 displays the ratio images from which the spectral indices were extracted and used for detection and identification. The value of multiple spectral indices lies in the fact that each spectral band ratio displays distinctive properties of different plastics, which can then be combined for classification. In other words, when each band ratio image is analyzed, it can be seen that different plastics are highlighted as bright versus dark areas depending on the ratio or index.

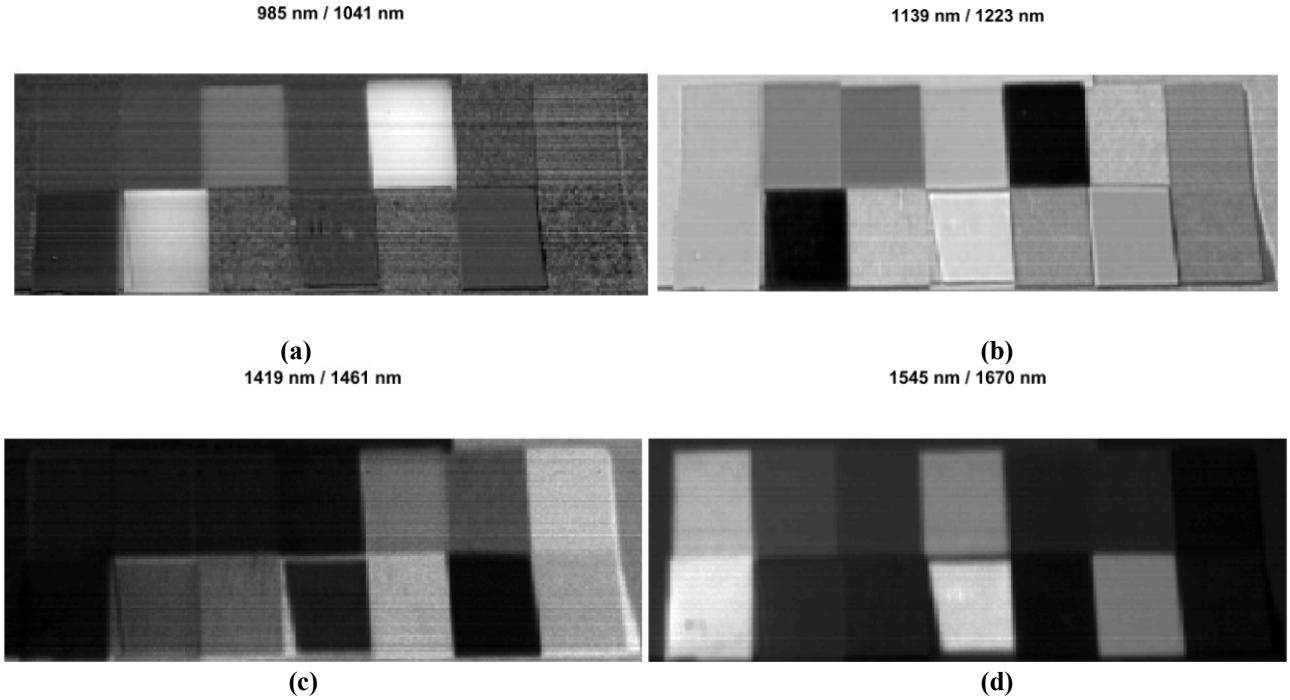

Figure 4. Images representing four band ratios. (a) $ratio_1$ = 985:1041; (b) $ratio_2$ = 1139:1223; (c) $ratio_3$ = 1419:1461; (d) $ratio_4$ = 1545:1670.

Figure 5 demonstrates the separability of tested plastic materials based on the three out of four band ratios selected and acquired from independent hyperspectral data cubes of each plastic sample. Only three band rations are displayed due to the limitation of 3D spatial plots. The feature values represented in the scatter plot come from Figures 3 and 4 at multiple (500) pixel locations for each material. Figure 5 shows the separability of plastic materials using the selected spectral indices. Some overlap exists between PVC (black) and HDPE (black), as well as between PETG (clear) and Kydex Acrylic PVC (gray). These two groups are plotted separately in Figure 6 to qualitatively visualize the extent of overlap in Figure 5. LPDE (white) shows the highest separability followed by HDPE (white) and PP (white). Polyester (white), PEEK (tan) and PS (white) are clustered in the same feature spatial proximity, but show clear between-class separability. PS (amber) and PC (clear) also appear close in the feature space but display between-class separability. High-temperature CPVC is clustered in the same feature space as Kydex Acrylic PVC (gray), and PETG (clear) as well as HDPE black. However, the clustering shows between-class separability of the high-temperature CPVC. In addition to the displayed feature space in 3D, the fourth band ratio is expected to alleviate some of the overlaps due to the above-mentioned materials.

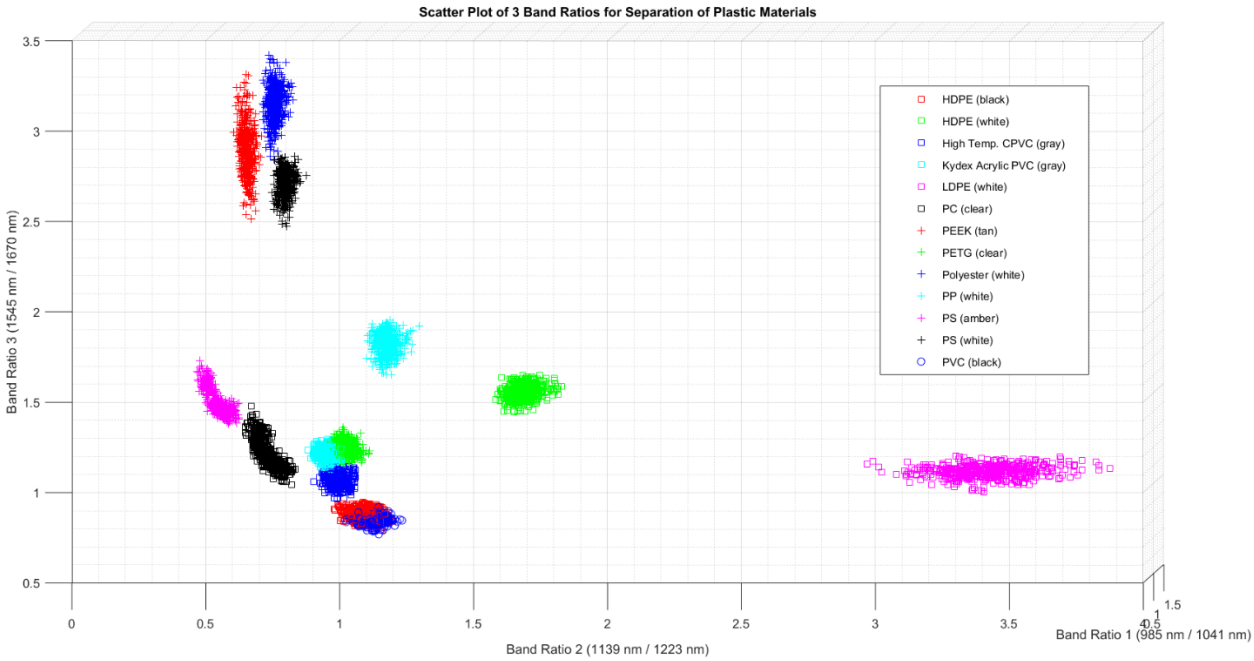

Figure 5. Clustering and separability of 13 plastic samples' band ratios (spectral indices) from average modified reflectance spectra represented in Fig. 3. Spectral indices were computed from individual samples in Table 1 and Figure 1.

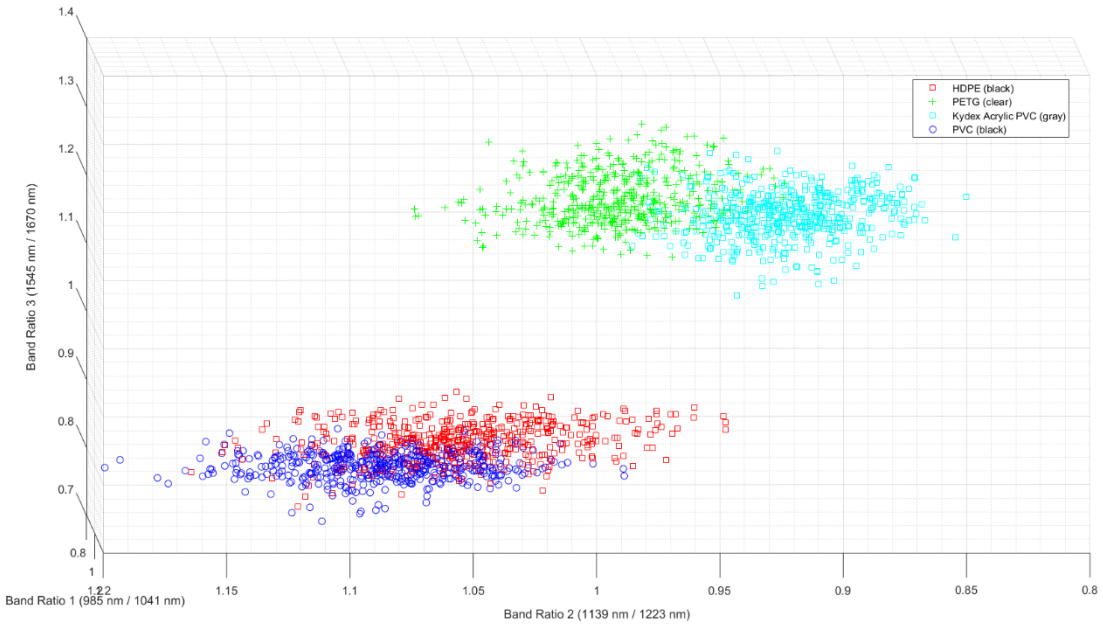

Figure 6. Two plastic pairs with overlapping features. Overlap between HDPE black and PVC black (bottom two clusters), and PETG (clear) and Kydex Acrylic PVC gray (top two clusters) reduces separability of the classes, and may cause misclassification. Fourth feature (not shown) is used to alleviate the overlap problem.

Figure 7 displays (a) a single test hyperspectral image frame and (b) semantic map based on classification and semantic segmentation results. The results are obtained from the SWIR hyperspectral image scene containing multiple plastic samples previously shown using digital color photography in Figure 2. This independent scene was not used during feature extraction shown in the scatter plots and spectral index images.

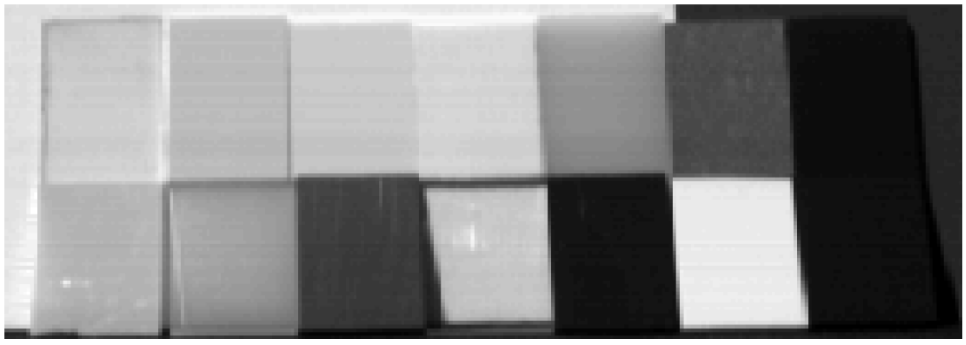

(a)

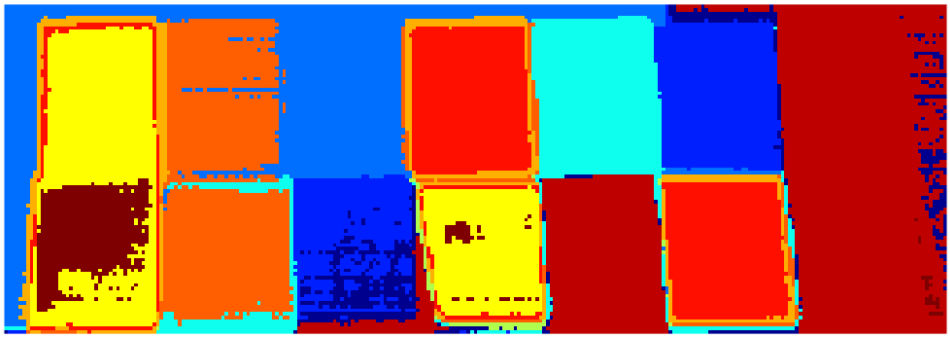

(b)

Figure 7. (a) Independent scene with different plastic samples extracted from hyperspectral data cube (frame 50, band 1041 nm, selected for demonstration purposes); (b) Initial mapping of plastics to the scene based on classification results.

As can be seen in Figure 7, nine different classes are visible among the plastic samples. The two PVC (black) samples in the scene (row 1, sample 7, and row 2, sample 5) are correctly identified. HDPE (black) (row 2, sample 7) has been classified in the same category as PVC (black) (row 1, sample 7). This can be explained based on the high similarity demonstrated in the scatter plots of Fig. 6, where the spectral indices forming the feature vectors demonstrated overlap. HDPE (white) (row 1, sample 3) was correctly identified. In this scene this material showed similarities with the background white screen, which was also classified as HDPE (white). It is possible that the background screen belonged to the same plastic category. PETG (clear) (row 1, sample 1) was distinctly identified, but showed partial similarity to PC (clear) (row 2, sample 4). This is a surprising result because the scatter plots show effective separability between these two classes. The error could possibly be due to 3D spatial symmetry of the tested feature vector in Euclidean distance to both clusters, which may render the D_E value closer to another cluster, if features happened to be close to cluster boundaries, for instance. PP (white) (row 1, sample 2) and LDPE (white) (row 2, sample 2) were classified as the same which was also surprising and requires further investigation. Polyester (row 1, sample 4) was correctly and uniquely identified. Kydex PVC (gray) (row 1, sample 6) was correctly identified but showed partial similarity to high-temperature CPVC (row 2, sample 3), which was also gray. PE (row 1, sample 5), which was not one of the thirteen samples in Table 1, was identified as a different material. PEEK (tan) (row 2, sample 1) was generally correctly identified, with some similarities to PETG (clear) (row 1, sample 1) and PC (white) (row 2, sample 4). Overall, out of the 14 samples present in the scene, including one that was not included in the original training, 10 were correctly classified using this simple distance metric.

5. CONCLUSION

Thirteen different plastic samples typically found in everyday use and general plastic waste were studied using SOC710-SWIR hyperspectral imaging system. Their separability was demonstrated using the hyperspectral image data and spectral indices as features. Some classification overlap existed in the final classification and mapping of the plastics. It is expected that some spectral mixing occurs due to spectral reflection from the samples that might result in slightly mixed pixels that might shift some spectral peaks. Shadows also affected the accuracy of the semantic map. Such discrepancies can be reduced with other image processing and classification schemes.

The SWIR region of the electromagnetic spectrum allows the capture of features not visible in the visible spectral range making this technology valuable for detecting materials that may have similar visual properties. The tested plastics were made of different materials and colors. Hyperspectral imaging continues to present itself as a viable imaging solution for detection and identification of plastics. SWIR HSI, in particular, shows the feasibility of this technique in identifying plastics in natural settings which is important for detection of plastic debris in terrestrial as well as marine environments. A successful detection and identification system requires proper coupling with classification algorithms for semantic segmentation and mapping that are implemented in software. The more recent deep learning and related algorithms show the potential for identifying a multitude of objects in both natural and laboratory environments, but require significant amounts of data for training, and represent ongoing work.

ACKNOWLEDGMENT

This project is an extension of the work performed as part of a grant from Texas A&M University-Corpus Christi - TCRF: *Integrated Characterization and Simulation System for Microplastics in Coastal Watersheds.* The authors thank Leif Hendricks for his valuable comments.

REFERENCES

[1] Jambeck, J. R., Geyer, R., Wilcox, C., Siegler, T. R., Perryman, M., Andrady, A., Narayan, R., and Law, K. L., "Plastic waste inputs from land into the ocean," Science, 347(6223), 768-769, (2015).
[2] "The new plastics economy: rethinking the future of plastics," World Economic Forum, 2016, 1-36 (January 2016). http://www3.weforum.org/docs/WEF_The_New_Plastics_Economy.pdf
[3] Carbery, M., O'Connor, W., and Thavamani, P., "Trophic transfer of microplastics and mixed contaminants in the marine food web and implications for human health," Environment International, 115, 400-409 (2018).
[4] Wang, W., Gao, H., Jin, S., Li, R., and Na, G., "The ecotoxicological effects of microplastics on aquatic food web, from primary producer to human: A review," Ecotoxicology and Environmental Safety, 173, 110-117 (2019).
[5] Limonta, G., Mancia, A., Benkhalqui, A., Bertolucci, C., Abelli, L., Fossi, M. C., and Panti, C., "Microplastics induce transcriptional changes, immune response and behavioral alterations in adult zebrafish," Scientific Reports, 9, 15775 (2019).
[6] Jin, Y., Lu, L., Tu, W., Luo, T., and Fu, Z., "Impacts of polystyrene microplastic on the gut barrier, microbiota and metabolism of mice," Science of the Total Environment, 649, 308-317, (2019).
[7] Shim, W. J., Hong, S. H., and Eo, S. E., "Identification methods in microplastic analysis: a review," Analytical Methods, 9, 1384-1391 (2016).
[8] V. Hidalgo-Ruz, L. Gutow, R. C. Thompson, M. Thiel, "Microplastics in the marine environment: A review of the methods used for identification and quantitation," Environmental Science & Technology, 46, 3060-3075 (2012).
[9] Löder, M. G. J. and Gerdts, G., "Methodology used for the detection and identification of microplastics – a critical appraisal," Marine Anthropogenic Litter, Ed. M. Bergmann, L. Gutow, M. Klages, 201-228 (2015).
[10] Tagg, A. S., Sapp, M., Harrison, J. P., and Ojeda, J. J., "Identification and quantitation of microplastics in wastewater using focal plan array-based reflectance micro-FT-IT imaging," Analytical Chemistry, 87, 6032-6040 (2015).
[11] Li, J., Liu, H., Chen, J. P., "Microplastics in freshwater systems: A review on occurrence, environmental effects, and methods for microplastic detection," Water Research, 137, 362-374 (2018).
[12] Karlsson, T. M., Grahn, H., van Bavel, B., and Geladi, P., "Hyperspectral imaging and data analysis for detecting and determining plastic contamination in seawater filters," Journal of Near Infrared Spectroscopy, 24, 141-149 (2016).

[13] Shan, J., Zhao, J., Liu, L., F. Wu, X. Wang, "Simple and rapid detection of microplastics in seawater using hyperspectral imaging technology," Analytica Chimica Acta, 1050, 161-168 (2019).
[14] The 5 Most Common Plastics & Their Everyday Use. https://www.cutplasticsheeting.co.uk/blog/uncategorized/the-5-most-common-plastics-their-everyday-uses/ (last accessed: 6-18-2020)
[15] Serranti, S., "Plastic waste monitoring and recycling by hyperspectral imaging technology," Proc. SPIE 11197, SPIE Future Sensing Technologies, 1119706 (November 2019). https://doi.org/10.1117/12.2549670
[16] Hibbitts, C. A., Bekker, D., Hanson, T., Knuth, A., Goldberg, A., Ryan, K., Cantillo, D., Daubon, D., and Morgan, F., "Dual-band discrimination and imaging of plastic objects", Proc. SPIE 11012, Detection and Sensing of Mines, Explosive Objects, and Obscured Targets XXIV, 1101211 (22 May 2019). https://doi.org/10.1117/12.2519014
[17] Balsi, M., Esposito, S. and Moroni, M., "Hyperspectral characterization of marine plastic litters," 2018 IEEE International Workshop on Metrology for the Sea; Learning to Measure Sea Health Parameters (MetroSea), Bari, Italy, 28-32 (2018). doi:10.1109/MetroSea.2018.8657875
[18] Serranti, S., Fiore, L., Bonifazi, G., Takeshima, A., Takeuchi, H., and Kashiwada, S., "Microplastics characterization by hyperspectral imaging in the SWIR range," Proc. SPIE. 11197, SPIE Future Sensing Technologies (Nov. 2019).
[19] G. Bonifazi, M. D'Agostini, A. Dall'Ava, S. Serranti, F. Turioni, "A new hyperspectral imaging based device for quality control in plastic recycling," Proc. SPIE. 8774, 87741M 1-13, Optical Sensors (2013).
[20] Moroni, M., Mei, A., Leonardi, A., Lup, E., and La Marca, F., "PET and PVC Separation with Hyperspectral Imagery," Sensors, 15, 2205-2227 (2015). doi:10.3390/s15010205
[21] Moroni, M. and Mei, A. "Characterization and Separation of Traditional and Bio-Plastics by Hyperspectral Devices," Appl. Sci., 10(2800) 1-19 (2020). https://doi.org/10.3390/app10082800
[22] Caballero, D., Bevilacqua, M., and Amigo, J. M., "Application of hyperspectral imaging and chemometrics for classifying plastics with brominated flame retardants," J. Spectral Imaging, 8(a1), 1-16 (2019).
[23] Zhang, Y., Wang, X., Shan, J., Zhao, J., Zhang, W., Liu, L., and Wu, F., "Hyperspectral imaging based method for rapid detection of microplastics in the intestinal tracts of fish," Environ. Sci. Technol., 53(9), 5151-5158 (2019). https://doi.org/10.1021/acs.est.8b07321
[24] Chaczko, Z., Wajs-Chaczko, P., Tien, D., and Haidar, Y., "Detection of microplastics using machine learning," 2019 International Conference on Machine Learning and Cybernetics (ICMLC), Kobe, Japan, 1-8 (2019). doi:10.1109/ICMLC48188.2019.8949221
[25] Surface Optics Corporation, SOC 710 Series Hyperspectral Imaging Systems. https://surfaceoptics.com/products/hyperspectral-imaging/soc710-portable-hyperspectral-camera/ (last accessed: 07/31/2020).
[26] Cope Plastics, Inc., Engineering materials, Products and applications guide, updated January 2018. https://pdf4pro.com/cdn/products-amp-applications-guide-cope-plastics-220784.pdf
[27] Professional Plastics, Inc., Acronyms for Plastics – (abbreviations). https://www.professionalplastics.com/ACRONYMS (last accessed: 7/22/2020).
[28] Mehrubeoglu, M., Zemlan, M. and Henry, S, "Hyperspectral imaging for differentiation of foreign materials from pinto beans," Proc. SPIE Optics + Photonics Conf., Optical Engineering + Applications, San Diego, CA, vol. 9611, Paper 96110A (2015). https://doi.org/10.1117/12.2207797